






Strain Effects of Absorbing Layer on Superconducting Properties of a High-Flux Neutron Detector

Mette Bybjerg Brock , Chung-Chuan Lai , Asger B. Abrahamsen , Linda Robinson, Kalliopi Kanaki, Richard Hall-Wilton, Anders C. Wulff , and Luise Theil Kuhn 

Abstract—An increasingly unstable supply of ^3He in the past decade along with growing demands for detectors from the large-scale neutron facilities have led to a higher focus on developing neutron detectors not relying on ^3He . In this study a superconducting transition edge sensor (TES) based on a stack of thin films is combined with a neutron absorbing layer of $^{10}\text{B}_4\text{C}$ to build a sensitive and robust neutron detector. The difference in lattice structure causes tensile strain in the thin, stacked, structure, which results in changes in the superconducting parameters. The strain was measured along with its effect on the superconducting transition and thereby the sensitivity of the detector. A decrease in T_c of a few percent and in the range of 0.3 to 2.2 K was found from two different samples with varying boron coverage for a calculated strain of $< 0.07\%$. A change in sensitivity due to strain was found to be from -58 to -15% , depending on deposition coverage and the deposition process. Effects on the superconducting properties were found to be within a range that can be compensated by design and setup considerations and these are therefore not expected to pose problems for the future detectors build on this principle.

Index Terms—Boron carbide, superconducting transition temperature, superconducting devices, tensile strain.

I. INTRODUCTION

IN THE past decades the supply of ^3He has become unstable due to its close relations to defense and security. At the same time neutron detector requirements have changed as faster and brighter sources are being installed at the large-scale neutron facilities around the world. Due to

Manuscript received September 28, 2021; revised December 10, 2021; accepted January 12, 2022. Date of publication January 25, 2022; date of current version March 9, 2022. (Corresponding author: Mette Bybjerg Brock.)

Mette Bybjerg Brock and Luise Theil Kuhn are with the DTU Energy, Technical University of Denmark, 2800 Kgs. Lyngby, Denmark (e-mail: mebyb@dtu.dk).

Chung-Chuan Lai and Linda Robinson are with ESS - European Spallation Source ERIC, 582 13 Linköping, Sweden.

Asger B. Abrahamsen is with DTU Wind Energy, Technical University of Denmark, 4000 Roskilde, Denmark.

Kalliopi Kanaki is with ESS - European Spallation Source ERIC, 224 84 Lund, Sweden.

Richard Hall-Wilton is with ESS - European Spallation Source ERIC, 224 84 Lund, Sweden and also with the Università degli Studi di Milano-Bicocca, 20126 Milano, Italy.

Anders C. Wulff is with the Subra A/S, 3520 Farum, Denmark.

Color versions of one or more figures in this article are available at <https://doi.org/10.1109/TASC.2022.3145322>.

Digital Object Identifier 10.1109/TASC.2022.3145322

^3He based detectors being the vast majority of existing neutron detectors, this has led to a stronger focus on developing novel neutron detectors based on other detection methods and materials.

There are only five materials with neutron absorption cross sections sufficiently high for use in effective neutron detection. These are ^3He , ^6Li , ^{10}B , ^{157}Gd and ^{113}Cd . ^6Li is often used for scintillator type detectors as described by N. J. Rhodes [1]. ^{157}Gd and ^{113}Cd have high cross-sections, but also exerts γ products from the absorption reaction. This is not ideal as superconducting detectors are known to be γ -ray sensitive. ^{10}B is currently being used in several new solid-state and combined gas and solid-state detector projects and constitute the neutron sensitive material in half of the new detector projects at the European Spallation Source (ESS) [2].

For these investigations, a superconducting transition edge sensor (TES) is paired with a neutron sensitive layer made of isotope enriched boron carbide in order to become neutron sensitive. The working hypothesis is that it is possible to transfer the well-described attractive abilities of high sensitivity, efficiency and resolution of a TES to the field of neutron detection, which could yield a new high-flux, high spatial resolution counter for neutron science applications.

Existing superconducting detectors for neutron detection are relatively few and so far non-commercial. Merlo *et al.* have tested a design with a ^{10}B -coated Nb and NbN nanostrip, which showed a very long reset time of 120s, far from the state-of-the-art of ms[3]. Yoshioka *et al.* developed a MgB_2 -based kinetic inductance detector (KID) using a meander design[4] and most recently, Iizawa *et al.* have developed the Nb-based Current Biased KID (CB-KID) as a functioning neutron imaging system[5]. The approach for the new bolometer aims to use a superconducting material operating at a higher transition temperature (T_c) to create a system easier to operate at a larger scale.

This investigation aims to quantify the effects on its superconducting properties caused by depositing a detector-grade layer of enriched boron carbide directly on top of a superconducting pixel structure used for a TES detector. The change in transition temperature and slope caused by the strain imposed in the stacks due to the deposited absorption layer has been

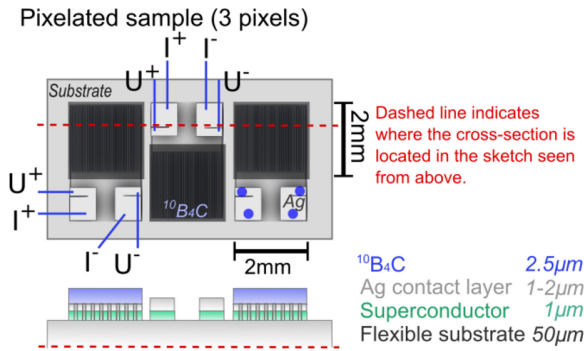


Fig. 1. Overview of the sample structures, sizes and geometry of deposited boron carbide: Drawing of sample types and the approximate placement of the electrical contacts. Dark grey areas mark boron carbide depositions. The stack structure is shown in the bottom of the figure. Dashed line indicates where in the above sketch, the cross-section of the stack structure is shown for.

investigated through measuring the normal-to-superconducting transition.

II. EXPERIMENTAL

A. Sample Preparation

Two pixelated samples were used for the electrical transport measurements, while a separate type was used for strain estimations. An overview of the geometry of the samples used for transport measurements can be seen in Fig. 1. The pixelated samples have $2 \times 2 \text{ mm}^2$ pixels, which have boron carbide deposited on top of either two (sample B2-pix Y, $Y = 1-3$) or all three pixels (sample B3-pix Y). The superconducting meander pattern constituting the pixel is $2 \times 2 \text{ mm}^2$ and is fully covered by boron carbide. Due to a fabrication error, the Ag contact layer covered the entire meander pattern, leading to a secondary current pathway, but without short-circuiting the individual lanes. The samples have the superconducting layer electrically isolated from the substrate by thin, non-conducting, intermediate layers. The Ag contact layer is deposited directly on top of the superconducting layer with no isolation layer in between. The superconducting material in the samples is a ceramic superconductor of a type similar to that used in [6].

Deposition on the samples was performed using shadow masks designed to cover the $2 \times 2 \text{ mm}^2$ pixels.

B. $^{10}\text{B}_4\text{C}$ Deposition

The $^{10}\text{B}_4\text{C}$ thin films were deposited by direct-current magnetron sputtering (DCMS) at ESS Detector Coatings Workshop. The deposition was performed with a commercial CC800/9 deposition system (CemeCon AG, Germany) following a well-described process for $^{10}\text{B}_4\text{C}$ neutron detector applications [7]–[9].

The samples were mounted horizontally facing toward a $90 \times 500 \text{ mm}^2$ $^{10}\text{B}_4\text{C}$ sputtering target (99.9% purity, RHP Technology GmbH, Austria) at a distance of 70 mm. The system was pumped to a base pressure of $2.5 \cdot 10^{-4} \text{ Pa}$, while the samples were heated to $100 \text{ }^\circ\text{C}$ for 10800 s to remove water from the surfaces. Thereafter, a 600 s plasma cleaning in 0.35 Pa

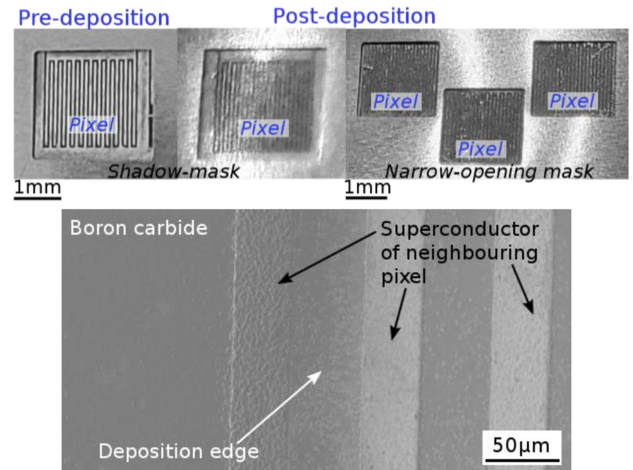


Fig. 2. Top: Photograph of a pixel before and after deposition having surrounding area covered by a $50\text{-}\mu\text{m}$ -thick shadow-mask. The 3-pixel post deposition to the right shows a mask design with narrower openings. Bottom: SEM image of deposition edge. Because of the wide opening mask design the edge of deposition coincides with the outermost of the neighboring pixel.

pure Ar atmosphere was performed to further reduce the oxide layers from the surface as well as to increase the geometrical roughness to improve the adhesion. An SRIM simulation [10] of ion damage in a $1 \text{ }\mu\text{m}$ thick superconductor with 650 eV Ar ions showed a stopping range of only 13 \AA , suggesting that the plasma cleaning step will not significantly damage the superconductor.

Prior to the $^{10}\text{B}_4\text{C}$ deposition, the chamber was filled with 0.3 Pa pure Ar gas. The target was supplied with a constant power of 1000 W for 25000 s during the deposition and the substrates were kept at a floating potential. Masks were attached during the entire procedure, so only areas meant for coating were exposed to the plasma cleaning as well as deposition. After the deposition, the samples were packed with silica gel bits for the transportation to DTU for further characterization.

C. Thickness Measurements

The thickness of the $^{10}\text{B}_4\text{C}$ films was measured by a Bruker DektakXT profilometer on the step-height of a thickness reference sample. The reference samples were mounted on an equivalent position in the same deposition runs with the superconducting samples. The deposited layer had a thickness of $2.5 \text{ }\mu\text{m}$ for non-masked samples. The thickness measured on the reference sample was $2.69 \text{ }\mu\text{m}$ in the middle of the plate and gradually decrease to $2.39 \text{ }\mu\text{m}$ when moving outward over a distance of 4 cm. This thickness gradient is expected to be mirrored in the horizontal direction due to the target geometry.

The small samples shown in Fig. 1 were mounted in $50 \text{ }\mu\text{m}$ thick shadow mask prior to deposition. Fig. 2 shows a pixel with the mask before and after the deposition. It also shows the narrow design used for a 3-pixel deposition in order to allow for a non-coated bridge between the $^{10}\text{B}_4\text{C}$ coated pixels. This gap in deposited $^{10}\text{B}_4\text{C}$ is made to lessen thermal cross-talk between pixels. The SEM image in the bottom of Fig. 2 shows a close-up of the edge of the deposited layer. Due to using a

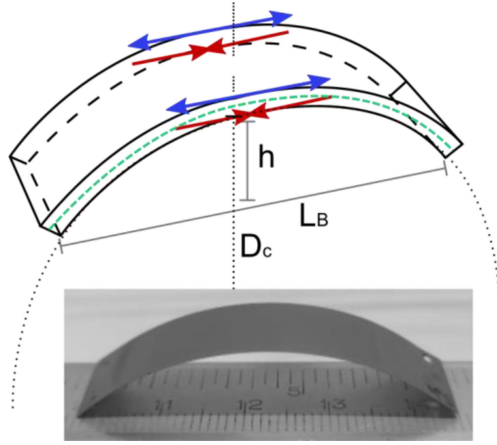


Fig. 3. Sketch and photo of the straining of a thin strip. Arrows indicate tension (blue) and compression (red). The green line indicates the neutral axis of the coated conductor. (Drawing based on [11]).

wide mask opening design, the superconducting structure of the neighboring pixel is just visible on the edge of the deposition.

D. Strain Analysis

The strain asserted on the superconducting layer due to deposition of $^{10}\text{B}_4\text{C}$ by DCMS was investigated using larger trial samples of length 49 mm of a similar superconducting thin film structure as the small samples. The long strips have $^{10}\text{B}_4\text{C}$ deposited over the entire superconducting area. The superconductor samples were flat prior to deposition, and therefore all curvature is assumed due to the deposition. The curved sample can be seen in Fig. 3.

The strain, ϵ_t , of the trial sample due to deposition was only found to affect the long direction and can therefore be described as the bending of a thin beam. The strain is therefore described as,

$$\epsilon_t = \frac{\pm d}{R_c}, \quad (1)$$

where d is the distance from the superconducting layer to the neutral axis and R_c is the radius of curvature for the sample measured from the neutral axis [11]. The sign of d is given by the strain being tensile (+) or compressive (-). The bending is sketched in Fig. 3.

The substrate in these superconducting samples makes up $\sim 95\%$ of the total thickness of the stack, and is nearly symmetric around the center line of the substrate. The neutral axis is therefore estimated as the center plane of the substrate.

The radius of curvature to the neutral axis is found as the sum of the radius of curvature measured beneath the sample, D_c , and the length from the bottom of the sample to the neutral axis, which is half the thickness of the substrate, t_{sub} ,

$$\epsilon_t = \frac{\pm d}{t_{sub}/2 + D_c}. \quad (2)$$

The radius of curvature as measured from the bottom of the sample can be found from the horizontal length underneath the curved sample, L_B , and the height from the curved sample to a

TABLE I
MEASURED LENGTHS AND CALCULATED STRAIN

Sample	Length (mm)	L_B (mm)	h (mm)	D_c (mm)	ϵ_t
A	49±1	45±1	8.5±0.5	34±2	0.073±0.004%
B	49±1	45±1	8.8±0.5	33±2	0.075±0.004%

Measured lengths of trial sample: full flat length, length when bend (L_B), height above horizontal axis (h), radius of curvature as measured from the bottom of the sample (D_c), and strain calculated using (3), and strain calculated using (1)

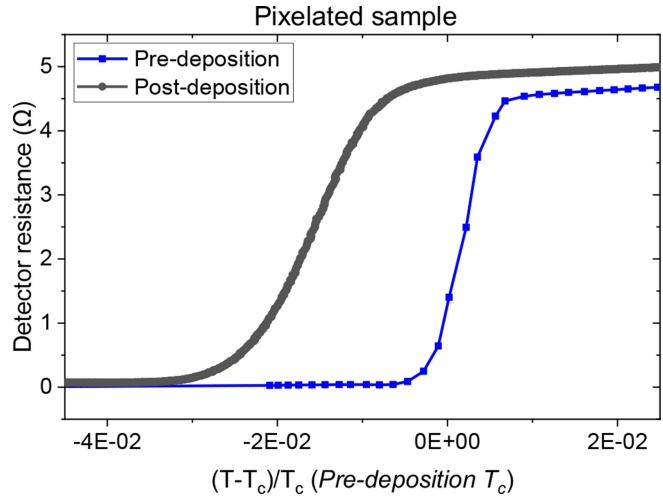


Fig. 4. Representative example of a superconducting transition measured for B3-pix1, a pixelated sample. Data shows a clear decrease in both T_c and the slope dR/dT .

flat surface underneath, h . The relation is given as

$$D_c = \frac{L_B^2 + 4h^2}{8h}. \quad (3)$$

The measured lengths of trial samples, calculated radius of curvature and in-plane strain can be seen in Table I, using $t_{sub} = 50 \mu\text{m}$ and $d = t_{sub}/2$.

E. Transport Measurements

In order to test for a change in superconducting properties, a temperature-resistance curve of the superconducting transition was measured prior to and after deposition for each pixel. An example of the superconducting transition curves measured for a pixelated (B3-pix1) sample is shown in Fig. 4.

The measurement was performed in a cryogenic environment ramping the temperature below and above the critical temperature, T_c . The temperature was monitored by a thermometer placed close to the sample holder. The resistance of the superconductor was measured by 4-point measurements with measuring currents of 10-20 μA for the pixelated samples. The magnitude of currents are chosen to avoid self-heating due to joule heating yet provide a reliable read-out signal.

Measurements have been performed on four pixels distributed on two pixelated samples. The measured changes in T_c and slope dR/dT of the superconducting transition for the pixelated

TABLE II
CHANGE IN TRANSITION TEMPERATURES AND SLOPES

Sample	ΔT_c (K)	$\Delta dR/dT$	$\Delta\%dR/dT$
B3-pix1	-1.5±0.2	-3.6±0.5 Ω/K	-54%
B3-pix2	-1.6±0.15	-4.67±0.09 Ω/K	-58%
B3-pix3	-2.2±0.15	-3.4±0.2 Ω/K	-61%
B2-pix1	-0.3±0.2	-1.2±1.5 Ω/K	-15%

Change in T_c and dR/dT values post boron carbide deposition on the pixelated samples. Uncertainty calculated as accumulated standard errors from averaging all measurements of a given sample.

samples are shown in Table II. The critical temperature T_c is defined as 50% of the normal resistance above the transition. The numeric value of the transition temperature is >8 K. The number of measurements for the transition of each sample ranges from two to seven and the uncertainty is calculated as the accumulated standard error found from averaging all measurements of a given sample.

III. DISCUSSION

The calculated strain of 0.07% is found for a long sample, which has full $^{10}\text{B}_4\text{C}$ coverage. The small samples for which electrical transport measurements were carried out were of smaller dimensions and only partly covered by $^{10}\text{B}_4\text{C}$ (Fig. 1). This difference in coverage compared to substrate provides a more mechanically stable stack for the smaller samples, since a similar length of substrate with a smaller coverage would show less deformation per length. This would lead to a larger arc length (Fig. 3), thereby decreasing the relative strain on the small samples compared to the larger test strips

Previous investigations of strain effects in superconductors comparable to those used here found that an in-plane strain of 0.05% resulted in a change of $T_c = 0.1$ K [12] and a change of $T_c = 0.4$ K for an in-plane strain of 0.022% [13]. The changes of 1.5–2.2 K found in this study for sample B3-pixY (Y = 1–3) is higher, which indicates that the decrease in T_c might be caused in parts by exposure during the deposition and not only by the strain. B2-pix1 with a change in T_c of 0.3 K is made from the same stack materials, but with $^{10}\text{B}_4\text{C}$ deposition only on two out of three pixels. The smaller total deposited area compared to the B3 sample leads to less change in T_c due to smaller strain. Further investigations would be needed to find the exact correlation. The numeric value of the transition temperature is > 8 K, so the differences are not in a range, which poses a problem for the current cryogenic cooling possibilities.

From Table II, the superconducting transition slope dR/dT can be seen to decrease for pixelated samples. The numeric values of dR/dT are in the order of 2–8 Ω/K, which is three orders of magnitude lower than values measured in similar meander structures [6]. This is due to the secondary current path-way in the overlaying Ag meander and is therefore not comparable to the values of a final detector design.

For the fully covered, pixelated samples the slope is expected to decrease due to the effect of the tensile stress, which can be seen as a relative decrease of 50-60% for sample B3-pixY (Y = 1–3) and 15% for the sample B2-pix1.

With further development of the detector the pixel size will decrease, which will result in a further decrease in relative strain on each pixel due to the deposition area becoming smaller. Thereby the effects on the transition will also decrease.

IV. CONCLUSION

The deposition of a detector-grade enriched $^{10}\text{B}_4\text{C}$ layer by DCMS results in decreased T_c (0.3 K–2.2 K) and decreased dR/dT of the pixel-based TES samples. The lowered T_c is easily accounted for by current cryo-cooler technology. The decrease in transition slope will lead to a decrease in sensitivity, which needs further measurements in order to be quantified. A decrease in sensitivity can be accounted for by adapting thinner features in the superconducting pattern or by changing the relative thicknesses of $^{10}\text{B}_4\text{C}$, superconductor and substrates in the stack structure.

The slight degradation of the superconducting properties due to strain from the deposition of the neutron sensitive layer is not of a magnitude that is deemed a problem for future detector applications.

ACKNOWLEDGMENT

The authors would like to thank to the ESS Detector Coatings Workshop, Linkping, Sweden for performing the deposition.

REFERENCES

- [1] N. J. Rhodes, "Scintillation detectors," in *Neutron News*, Oxford, U.K.: Taylor & Francis, 2012.
- [2] K. H. Andersen *et al.*, "The instrument suite of the European Spallation Source," *Nucl. Instrum. Methods Phys. Res.*, vol. 957, p. 163402, 2020. doi: 10.1016/j.nima.2020.163402
- [3] V. Merlo *et al.*, "Hybrid superconducting neutron detectors," *Appl. Phys. Lett.*, vol. 106, 2015, Art. no. 113502.
- [4] N. Yoshioka *et al.*, "Current-biased kinetic inductance detector using MgB_2 nanowires for detecting neutrons," *IEEE Trans. Appl. Supercond.*, vol. 23, no. 3, Jun. 2013, Art. no. 2400604.
- [5] Y. Iizawa *et al.*, "Energy-resolved neutron imaging with high spatial resolution using a superconducting delay-line kinetic inductance detector," *Supercond. Sci. Technol.*, vol. 32, 2019, Art. no. 125009.
- [6] R. Nazifi *et al.*, "Millimeter-wave response of all metal-organic deposited YBCO transition edge bolometer," *IEEE Trans. Appl. Supercond.*, vol. 31, no. 1, Jan. 2021, Art. no. 2100105.
- [7] C. Höglund *et al.*, " B_4C thin films for neutron detection," *J. Appl. Phys.*, vol. 111, no. 10, 2012, Art. no. 104908.
- [8] C. Höglund *et al.*, "Stability of $^{10}\text{B}_4\text{C}$ thin films under neutron radiation," in *Radiation Physics Chemistry*, Amsterdam, The Netherlands: Elsevier, 2015.
- [9] S. Schmidt *et al.*, "Low-temperature growth of boron carbide coatings by direct current magnetron sputtering and high-power impulse magnetron sputtering," *J. Mater. Sci.*, vol. 51, no. 23, pp. 10418–10428, 2016.
- [10] J. F. Ziegler, M. D. Ziegler, and J. P. Biersack, "SRIM—The stopping and range of ions in matter," *Nucl. Instruments Methods Phys. Res. Sect. B: Beam Interact. Mater. At.*, vol. 268, pp. 1818–1823, 2010.
- [11] W. D. Markiewicz and C. A. Swenson, "Winding strain analysis for YBCO coated conductors," in *Superconductor Science Technology*, Bristol, U.K.: IOP, 2010.
- [12] R. Hühne *et al.*, "Dynamic investigations on the influence of epitaxial strain on the superconducting transition in $\text{YBa}_2\text{Cu}_3\text{O}_{7-x}$," *Supercond. Sci. Technol.*, vol. 21, no. 7, 2008, Art. no. 075020.
- [13] S. Trommler *et al.*, "Reversible shift in the superconducting transition for $\text{La}_{1.85}\text{Sr}_{0.15}\text{CuO}_4$ and $\text{BaFe}_{1.8}\text{Co}_{0.2}\text{As}_2$ using piezoelectric substrates," *New J. Phys.*, vol. 12, no. 10, 2010, Art. no. 103030.